Nucleic Acids Research, 1995, Vol. 23, No. 23 4793–4798

Transition state stabilization by the 'high' motif of class I aminoacyl-tRNA synthetases: the case of *Escherichia coli* methionyl-tRNA synthetase

Emmanuelle Schmitt, Michel Panvert, Sylvain Blanquet and Yves Mechulam*

Laboratoire de Biochimie, Unité de Recherche Associée no. 1970 du Centre National de la Recherche Scientifique, Ecole Polytechnique, F-91128 Palaiseau cedex, France

Received September 21, 1995; Revised and Accepted October 30, 1995

ABSTRACT

Methionyl-tRNA synthetase belongs to the class I aminoacyl-tRNA synthetase family characterized both by a catalytic center built around a Rossmann Fold and by the presence of the two peptidic marker sequences HIGH and KMSKS. In this study, the role of the $_{21}$HLGH$_{24}$ motif of *Escherichia coli* methionyl-tRNA synthetase was studied in a systematic fashion by site-directed mutagenesis. It is shown that the two histidine residues play a crucial role in the catalysis of the methionyl adenylate formation by participating in the stabilisation of the ATP phosphate chain during the transition state. Moreover, the results suggest the involvement of the ε-imino group of histidine 21 and of the δ-imino group of histidine 24. Notably, the substitution of either the leucine or the glycine residue of the HLGH motif by alanine had no effect on the catalysis. From the data and from other studies with class I aminoacyl-tRNA synthetases, concomitant positive contributions of the HIGH and KMSKS sequences to reach the transition state of aminoacyl adenylate formation can be envisaged.

INTRODUCTION

The specific reaction of aminoacylation of tRNAs catalyzed by aminoacyl-tRNA synthetases (aaRS) can be divided into two steps: the activation by ATP of the amino acid substrate to give an aminoacyl adenylate, and the subsequent transfer of the aminoacyl moiety onto the 3′ end of the tRNA. Although all known synthetases catalyse this same reaction, the specific enzymes display a broad structural diversity. Two basic classes of aaRS can be recognized, however (1,2). Class I aminoacyl-tRNA synthetases contain two consensus sequences, HIGH and KMSKS (3–5), which are typical of a catalytic center built around a Rossmann fold (6). The catalytic center of a class II aaRS is marked by the presence of three other motifs (called motifs 1, 2 and 3). This center is built around an antiparallel β-sheet (2,7).

In the nucleotide binding fold of class I aaRS, the KMSKS motif is surrounded by several basic residues and is located in a flexible region between the βE strand and the αF helix. With both TyrRS from *Bacillus stearothermophilus* and MetRS from *Escherichia coli*, the 3-D structures of which are known (8–10), the KMSKS consensus sequence was shown to be involved in the stabilisation of the transition state of the amino acid activation reaction (11–15). However, despite this conserved role of the KMSKS loop, the specific amino acid composition of this motif is markedly degenerate within the class I aaRS. This feature likely reflects the requirement of each enzyme species for a conserved catalytic function while allowing for differing binding and efficiency characteristics, as illustrated by the substitution of the KMSKS sequence of *E.coli* MetRS by the equivalent KFGKT one of *B.stearothermophilus* TyrRS which caused a marked destabilization of the transition state of the methionine activation reaction (15).

In several cases, site-directed mutagenesis was used to probe the importance of the two histidine residues composing the HIGH sequence, the second motif characteristic of class I aaRS. With *B.stearothermophilus* TyrRS, these residues establish hydrogen bonds with the ATP molecule during the catalysis of aminoacyl adenylate formation (16,17). The substitution of either of the two histidine residues with asparagine or glutamine allowed the identification of the hydrogen donors. With *B.stearothermophilus* ValRS, the upstream histidine of the motif plays a role identical to that observed with TyrRS (18). In the case of *E.coli* TrpRS, which has a TIGN sequence instead of the HIGH sequence, the threonine also appeared to be involved in transition state stabilization during the amino acid activation reaction (19).

The aim of the present study is to expand the above investigations to *E.coli* methionyl-tRNA synthetase by probing the structure-function relationships of each of the residues composing its HLGH motif. From the data, general conclusions are drawn on the mechanism of action of class I aaRS.

MATERIALS AND METHODS

Production by site-directed mutagenesis and purification of the MetRS variants

The procedure used to produce variants of the M547 monomeric form of MetRS was described elsewhere (20,15,21). The M547 variants were produced in JM101Tr cells (22) in the presence of isopropyl-β-D-thiogalactoside (0.3 mM), and purified to homo-

* To whom correspondence should be addressed

geneity as previously described (21,23). Enzyme concentrations were calculated using the specific extinction coefficient at 280 nm of the trypsin-modified MetRS (1.72cm^2/mg; 24).

Isotopic [^{32}P]PPi-ATP exchange measurements

Methionine-dependent [^{32}P]PPi-ATP exchange activity was measured at 25°C in standard buffer (20 mM Tris–HCl, 7 mM $MgCl_2$, 10 mM 2-mercaptoethanol, 0.1 mM EDTA, pH 7.6) containing 2 mM [^{32}P]PPi, 2 mM ATP and 2 mM methionine (25). For K_m measurements, the concentrations of ATP or methionine were varied in the above assay from 40 µM to 2 mM, or from 3 µM to 2 mM, respectively.

Fluorescence at equilibrium

Variations of the intrinsic fluorescence of M547 variants upon titration with substrates were followed as described (11,26–28), at 25°C, in 20 mM Tris–HCl (pH 7.6), 10 mM 2-mercaptoethanol, 2 mM $MgCl_2$ and 0.1 mM EDTA. Saturation curves were obtained by varying the total concentration of ligands: methionine, 0.1 µM to 1.9 mM; methioninol, 0.2 µM to 5.6 mM. The dissociation constant of ATP-Mg^{2+} from its complex with the enzyme could be drawn from the variation of the apparent dissociation constant of methioninol as a function of increasing concentrations of this nucleotide (from 25 µM to 10 mM) (28,29).

Dissociation constants were determined from iterative non-linear least-square fits of the theoretical equations (25,27–29) to the experimental values. Confidence limits and standard errors were determined by 100 Monte Carlo simulations from the experimental deviations on individual measurements (30).

Fluorescence at the pre-steady-state

The formation of methionyl adenylate and its pyrophosphorolysis cause large variations of the intrinsic fluorescence of MetRS, from which the kinetic and equilibrium constants defined in the scheme below can be derived (26,31).

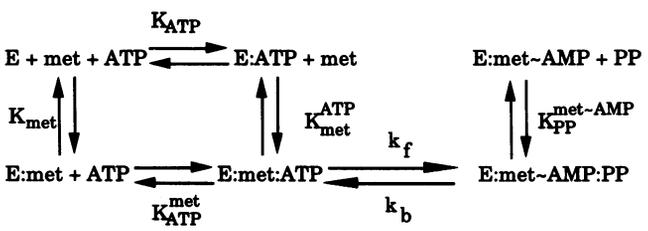

Fluorescence measurements at the pre-steady-state were performed using a Stopped Flow apparatus described in (31). All experiments were performed in 20 mM Tris–HCl (pH 7.6) containing 0.1 mM EDTA, 10 mM 2-mercaptoethanol and 2 mM free $MgCl_2$. The formation of methionyl adenylate was initiated by mixing (1:1 v/v) an enzyme solution (1.6 µM) containing methionine (1 mM) and a buffering pyrophosphate concentration (10 µM) with another solution containing the same concentrations of methionine and of pyrophosphate plus various amounts of the stoichiometric ATP-Mg^{2+} complex (0.2–20 mM). For the reverse reaction, the preformed enzyme–methionyl adenylate complex (obtained by incubating 1.6 µM enzyme in the presence of the concentrations of methionine and ATP-Mg^{2+} indicated in Table 3) was mixed 1:1 with a solution containing the same concentrations of methionine and ATP-Mg^{2+} plus various PPi-Mg^{2+} concentrations (0.05–4 mM).

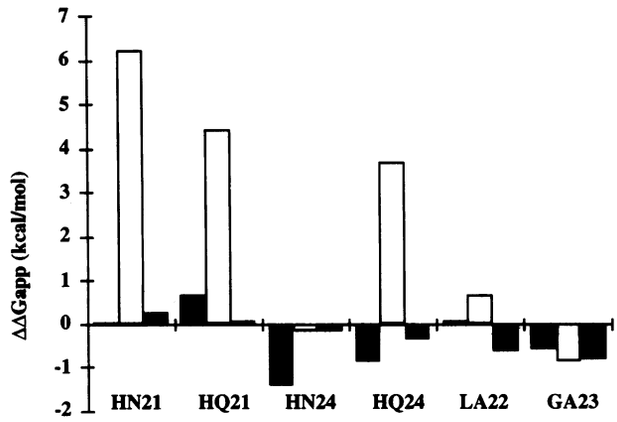

Figure 1. Difference free energy diagrams of the studied M547 variants. The difference free energies ($\Delta\Delta G_{app}$) for each state of the methionine activation reaction were calculated by substracting the free energy of the M547 enzyme from the free energy of the indicated mutant enzyme. Filled bars, E–met–ATP-Mg^{2+} complex; open bars, transition state; grey bars, E–methionyl adenylate complex. The values concerning E–methionyl adenylate–PPi-Mg^{2+} were omitted because in many cases the $K_{pp}^{Met\sim AMP}$ and the k_b values were not measurable.

Kinetic parameters (k_f and k_b) and equilibrium constants (K_{ATP}^{Met}, K_{met}^{ATP} and $K_{PP}^{met\sim AMP}$) of the methionine activation reaction (Scheme 1) are those defined in (31). Their values were drawn from fits of the measured rate constants to the theoretical equation (31).

RESULTS

Production and characterisation of the enzymatic variants

In order to probe the importance of the $_{21}$HLGH$_{24}$ motif of *E.coli* methionyl-tRNA synthetase, the corresponding residues were mutagenized. As previously proposed (16,17), the δ nitrogen of histidine is spatially analogous to the amide nitrogen of Asn and its ε nitrogen to the amide nitrogen of Gln. In order to evaluate the importance of both imino groups, each of the two histidine residues of the MetRS $_{21}$HLGH$_{24}$ sequence was substituted with either asparagine or glutamine. The resulting enzymatic variants, H21N, H21Q, H24N and H24Q were produced and purified. Finally, to study the two remaining positions of HLGH, leucine 22 was substituted with alanine (L22A variant) and glycine 23 with either alanine (G23A) or the bulkier proline (G23P).

The Michaelis–Menten parameters of the isotopic [^{32}P]PPi-ATP exchange reaction catalyzed by the seven purified enzymatic variants were measured (Table 1). It can be noted first that the rate (k_{cat}) of the isotopic exchange reaction was only slightly affected in the cases of the L22A and G23A variants. In contrast, substitution of G23 with proline reduced the rate of the isotopic exchange reaction by three orders of magnitude. Secondly, substitution of H21 with either glutamine or asparagine, as well as substitution of H24 with glutamine, decreased the catalytic efficiency (k_{cat}/K_m) of ATP-Mg^{2+} of the isotopic exchange reaction by a factor larger than three orders of magnitude. In

contrast, the H24N mutation affected the catalytic efficiency by only a factor of 6. It is worth noting that in all studied cases the reduction of catalytic efficiency reflected predominantly the lowering of the maximal rate (k_{cat}) of the isotopic exchange reaction. Whatever the enzyme variant, the net increase of the K_m value of ATP-Mg^{2+} never exceeded 7-fold and that of methionine never more than 1.6. These results suggest that the amino acid substitutions did, indeed, act at the level of the catalytic step and not through a structural disorganization of the catalytic centre.

Table 1. Michaelis–Menten parameters of the [^{32}P]PPi-ATP isotopic exchange reaction catalysed by MetRS variants

	K_{mATP} (μM)	k_{cat} (s^{-1})	relative k_{cat}/K_m[a]	K_{mMet}[b] (μM)
547	410 ± 50	55 ± 5	100	20 ± 2
H21N	300 ± 40	0.016 ± 0.001	0.05	6 ± 1
H21Q	2500 ± 1000	0.20 ± 0.07	0.07	33 ± 3
L22A	1100 ± 200	25 ± 2	21	32 ± 3
G23A	382 ± 46	60 ± 6	139	11 ± 1
G23P	393 ± 52	0.08 ± 0.01	0.18	10 ± 1
H24N	292 ± 34	5.4 ± 0.5	16	6 ± 1
H24Q	3000 ± 1000	0.2 ± 0.1	0.04	14 ± 1

[a]Given as percentages of the value determined for the M547 enzyme where K_m is that of ATP-Mg^{2+} measured in the presence of 2 mM methionine.
[b]K_m of methionine is measured in the presence of 2 mM ATP-Mg^{2+}.

The residues composing the HLGH motif are not involved in initial substrate binding

To continue analysis of the mutant enzymes, binding constants of methionine and ATP-Mg^{2+} were determined at equilibrium by spectrofluorimetric titrations. Because of its importance in the formation of the E–met–ATP-Mg^{2+} reactive complex, the strength of positive free energy coupling between the bindings of methionine (met) and ATP-Mg^{2+} to their sites was also examined. This energy coupling is believed to compensate for the repulsion expected from the negative charges carried by the carboxylate of methionine and the α-phosphoryl group of ATP and also to drive the substrates towards the transition state (28,29,31). To follow the effect of methionine site occupation on ATP-Mg^{2+} binding and vice versa, the free energy of coupling between the two sites can be measured by suppressing one of these two negative charges. For instance, methioninol can be used in place of methionine, or a combination of adenosine plus PPi-Mg^{2+} can mimic the ATP-Mg^{2+} molecule lacking the α-phosphate charge.

Equilibrium constants and coupling parameters are presented in Table 2. None of the substitutions performed in M547 had strong effects on the stability of the E–met or E–ATP-Mg^{2+} binary complexes. Further, for all studied variants except G23P, the coupling afforded by the occupation of the ATP-Mg^{2+} site to methioninol binding still occurred. Indeed, in the cases of the H24Q and H21N variants, the corresponding coupling free energy, C_{metol}^{ATP} as defined in Table 2, was decreased by at most 2 kcal/mol, as compared to the wild-type M547 enzyme. In contrast, while C_{met}^{ado} (the coupling free energy between the methionine and adenosine sites) was reduced with the G23P variant, the coupling between the PPi-Mg^{2+} and methionine sites, as measured in the presence of adenosine, disappeared when using the H21N, H21Q, H24Q and G23P variants, and was slightly lowered with L22A.

Table 2. Equilibrium constants for the formation of the binary enzymatic complexes and coupling parameters between the methionine, adenosine and PPi-Mg^{2+} sites

	K_{met}[a] (μM)	K_{met}^{ado} b (μM)	C_{met}^{ado} c (kcal/mol)	$K_{met}^{ado\text{-}PPi}$ d (μM)	$C_{met}^{ado\text{-}PPi}$ e (kcal/mol)	K_{metol}[f] (μM)	K_{metol}^{ATP} g (μM)	K_{ATP}[h] (mM)	C_{metol}^{ATP} i (kcal/mol)
547	38 ± 6	9 ± 1	**0.8**	0.65 ± 0.10	**1.5**	417 ± 85	1.7 ± 0.4	1.0 ± 0.8	**3.3**
H21N	60 ± 6	23 ± 3	**0.6**	21 ± 4	**0.06**	380 ± 20	23 ± 2	2.2 ± 0.4	**1.7**
H21Q	63 ± 9	11 ± 2	**1.0**	14 ± 2	**–0.1**	130 ± 10	3.5 ± 0.2	0.7 ± 0.1	**2.1**
L22A	35 ± 4	9.5 ± 1.0	**0.8**	1.55 ± 0.15	**1.1**	355 ± 40	4.7 ± 0.5	1.1 ± 0.2	**2.6**
H24N	41 ± 11	7 ± 1	**1.0**	0.5 ± 0.3	**1.6**	195 ± 10	0.5 ± 0.1	1.4 ± 0.3	**3.5**
H24Q	25 ± 3	3.0 ± 0.5	**1.2**	1.3 ± 0.2	**0.5**	310 ± 20	36 ± 2	1.0 ± 0.1	**1.3**
G23A	55 ± 6	10 ± 1	**1.0**	0.65 ± 0.10	**1.6**	350 ± 30	1.8 ± 0.2	0.8 ± 0.1	**3.1**
G23P	71 ± 10	45 ± 4	**0.3**	53 ± 6	**-0.1**	278 ± 15	115 ± 13	3.2 ± 2.0	**0.5**

Determination of these parameters was as described in Materials and Methods.
[a]K_{met} is the dissociation constant of the enzyme–methionine complex.
[b]K_{met}^{ado} is the apparent dissociation constant of methionine when measured in the presence of 14 mM adenosine.
[c]C_{met}^{ado} = RT Log(K_{met}/K_{met}^{ado}).
[d] $K_{met}^{ado\text{-}PPi}$ is the apparent dissociation constant of methionine when measured in the presence of 14 mM adenosine and 2 mM PPi-Mg^{2+}.
[e] C_{met}^{ado} = RT Log($K_{met}^{ado}/K_{met}^{ado\text{-}PPi}$)
[f]K_{metol} is the dissociation constant of methioninol from the enzyme–methioninol complex.
[g]K_{ATP} is the dissociation constant of the enzyme–ATP-Mg^{2+} complex.
[h] K_{metol}^{ATP} is the dissociation constant of methioninol from the enzyme–ATP-Mg^{2+}–methioninol complex.
[i]C_{metol}^{ATP} = RT Log($K_{metol}/K_{metol}^{ATP}$).

Each of the histidine residues are necessary for efficient catalysis

To analyze more precisely the role of each of the residues composing the $_{21}$HLGH$_{24}$ motif, rate constants of the methionine activation reaction were measured (Scheme 1). The values derived from the pre-steady-state analysis are summarized in Table 3 and in Figure 1. First, in agreement with the results of the [^{32}P]PPi-ATP isotopic exchange assay, modification of leucine 22 or glycine 23 by an alanine residue only slightly affected the thermodynamic parameters of the methionine activation reaction. However, it is notable that the affinity of PPi-Mg^{2+} for the E–met~AMP complex increased by one order of magnitude when using the L22A variant. On the other hand, when using the G23P variant, methionyl adenylate formation followed a biphasic kinetic. In this case, the small relative variation of the amplitude of fluorescence allowed only rough estimation of the rate constants. Nevertheless, rate values in the order of 1 s^{-1} for the rapid phase and of 0.05 s^{-1} for the slow phase clearly indicated that the G23P substitution has a major effect on enzyme catalysis.

The substitution of histidine 24 with an asparagine residue (variant H24N) moderately affected the rate of methionyl adenylate synthesis or the rate of its pyrophosphorolysis; k_f and k_b were reduced by factors of 10 and 2.5, respectively. In contrast, the k_f associated with the H24Q variant was drastically reduced (three orders of magnitude) when compared with M547. In the case of the reaction of pyrophosphorolysis of the adenylate, the dissociation constant of PPi-Mg^{2+} from the H24Q–met~AMP–PPi-Mg^{2+} complex was above the solubility of this ligand and so became immeasurably high (>5 mM). As a result, the rate of the backward reaction (k_b) could not be accurately determined. However, the k_b/K_{PP} ratio remained measurable and was found to be three orders of magnitude lower than that of the M547 control.

The substitution of histidine 21 with an asparagine (variant H21N) resulted in a larger reduction in the rate of methionyl adenylate synthesis (four orders of magnitude) than its substitution with a glutamine (three orders of magnitude). Further, as observed above with the H24Q mutant, the reduction of the forward rate constants were systematically paralleled by a weakened affinity of PPi-Mg^{2+} for the E–met~AMP complex. Finally, it is noteworthy that for all the studied H21 and H24 mutants, the value of the affinity of ATP-Mg^{2+} for the E–met complex was only slightly modified.

DISCUSSION

Substituting each of the two histidines belonging to the $_{21}$HLGH$_{24}$ motif of MetRS with either an asparagine or a glutamine led to the following effects on the catalysis of methionine activation. (i) Neither mutation of H21 or H24 impairs the binding of the methionine or ATP-Mg^{2+} substrates forming the ground-state E–met–ATP-Mg^{2+} complex, as clearly shown by the difference free energy plots at each step of the methionine activation reaction (Fig. 1). (ii) Substitution of H24 with an asparagine is nearly functionally conservative whereas its substitution with a glutamine strongly destabilises the transition state of the methionine activation reaction (3.6 kcal/mol). (iii) In the case of H21, both the H21N and H21Q mutations led to a marked increase in the free energy of transition state binding. However, the increase is equal to 6.2 kcal/mol with H21N and only 4.2 kcal/mol with H21Q. Therefore, in contrast to the situation observed with H24, the substitution of H21 with an asparagine is more detrimental to the catalysis than that with a glutamine. From this behaviour, two conclusions may be drawn. First, both histidine residues contribute to the stabilization of the transition state complex. Secondly, because the δ nitrogen of histidine is spatially analogous to the amide nitrogen of Asn while its ε nitrogen is mimicked by the amide nitrogen of Gln (17), the δ-imino group of H24 rather than the ε-imino one, should be hydrogen bonded to the transition state. Moreover, although the substitution of H21 with a glutamine is not conservative, the results favor the idea that the ε-imino group of histidine 21 is more important than the δ-imino group for an efficient catalysis.

Table 3. Thermodynamic and kinetic parameters of the methionine activation reaction

	k_f (s^{-1})[a]	K_{ATP}^{met} (mM)[a]	k_f/K_{ATP}^{met} ($s^{-1}M^{-1}$)10^{-3}	C_{ATP}^{met} [b] (kcal/mol)	k_b (s^{-1})[a]	$K_{PP}^{Met\sim AMP}$ (mM)[a]	$k_b/K_{PP}^{Met\sim AMP}$ ($s^{-1}M^{-1}$)10^{-3}[a]
M547	328 ± 30	1.0 ± 0.2	342 ± 51	0.0	181 ± 22	0.06 ± 0.02	3,700 ± 1,200
H21N	0.010 ± 0.001	1 ± 0.3	0.010 ± 0.002	0.5	nm[c]	>5	0.16 ± 0.01
H21Q	0.57 ± 0.06	2.6 ± 0.5	0.22 ± 0.02	–0.8	nm	>5	2.5 ± 0.1
L22A	120 ± 10	1.8 ± 0.3	67 ± 6	–0.3	393 ± 90	0.95 ± 0.3	410 ± 50
G23A	521 ± 35	0.38 ± 0.1	1390 ± 206	0.4	160 ± 10	0.07 ± 0.02	2,200 ± 300
H24N	39 ± 1	0.12 ± 0.01	320 ± 20	1.45	70 ± 5	0.02 ± 0.01	3780 ± 1050
H24Q	0.15 ± 0.01	0.5	0.30 ± 0.04	0.4	nm	nm	4.0 ± 0.2

[a]The values were derived from a pre-steady-state analysis by using a stopped flow apparatus. The catalytic parameters for the forward reaction were measured in the presence of a buffering concentration of pyrophosphate (10 μM), in excess with respect to the pyrophosphate produced during the reaction. For the backward reaction, the methionyl adenylate was preformed in the presence of 1 mM methionine and 0.05 mM ATP-Mg^{2+} with the G23A and H24N enzymes, 0.1 mM ATP-Mg^{2+} with the M547 and L22A enzymes, 0.2 mM ATP-Mg^{2+} with the H21Q and the H24Q and 1 mM ATP-Mg^{2+} with the H21N enzyme. The pyrophosphorolysis was then initiated by mixing 1:1 with a solution containing the same concentrations of methionine and ATP-Mg^{2+} as above plus various PPi-Mg^{2+} concentrations. For all measurements, free Mg^{2+} concentration, in excess of the sum of ATP and PPi concentrations, was maintained equal to 2 mM.

[b]$C_{ATP}^{met} = RT \ Log(K_{ATP}/K_{ATP}^{met})$.

[c]nm, not measurable.

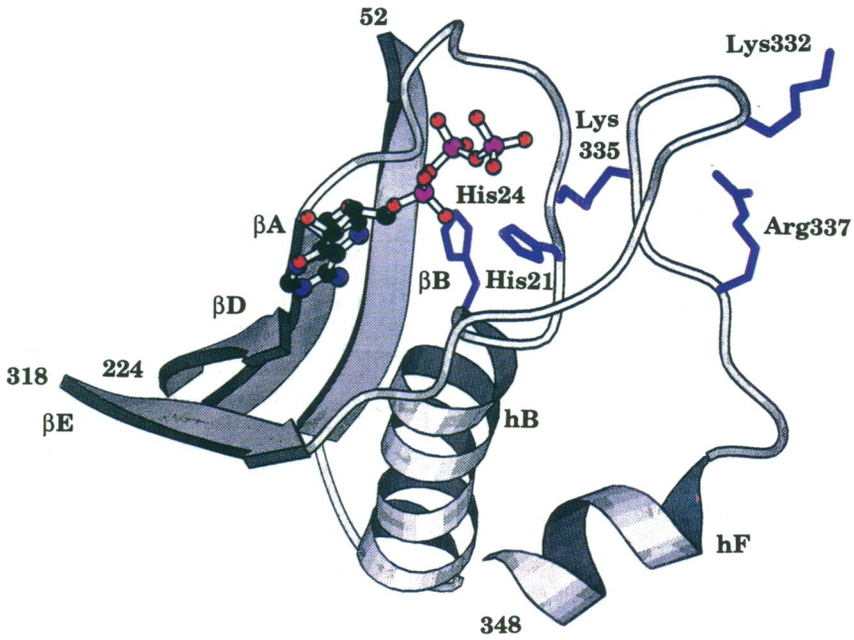

Figure 2. Schematic drawing of the ATP binding region of *E.coli* MetRS. Shown are the peptidic regions surrounding the ATP molecule: strand A, helix B and strand B (residues 6–52); strand D (residues 224–232) and strand E and helix F (318–348). The important residues in HLGH and KMSKS motifs (H21, H24, K332 and K335) as well as R337 are also noted. The ball-and-stick model represents the bound ATP molecule. The figure was drawn from the MetRS co-ordinates (10) using the program Molscript (36).

Examination of the three-dimensional structure of the MetRS–ATP complex (Fig. 2) shows that the ε-imino group of His21 is close (3.1 Å) to the phosphate chain of ATP (10). It can therefore be proposed that the phosphates of ATP are the target of His21 during the transition state. In terms of His24, its δ-imino group is located 5 Å from the O1 oxygen of the ribose. The α-phosphoryl oxygen of ATP is also near this imino group (4.6 Å). Either oxygen might therefore interact with His24 during formation of the transition state.

The conclusions regarding the role of the histidines within the HLGH motif of *E.coli* MetRS closely parallel those drawn from the study of the HIGH motif of *B.stearothermophilus* TyrRS (16,17) and of the upstream histidine of *B.stearothermophilus* ValRS (18). Similar conclusions were also drawn from analysis of the structure of the GlnRS–$tRNA^{Gln}$–ATP complex. Together, the whole data clearly indicate a conservation of the role of the two His of the HIGH motif within class I aaRS. In a few class I aaRS, an asparagine residue is found in place of the second histidine within the HIGH motif (see a compilation of the corresponding sequences in 32). This asparagine is likely to fulfill the role of the δ-imino group of a histidine at this position (these results and 16). Moreover, in the case of the *E.coli* tryptophanyl-tRNA synthetase, which displays a TIGN sequence instead of HIGH, the threonine residue was found to play a role similar to that of the corresponding histidine (16).

In the case of *E.coli* MetRS, the two other residues composing the HLGH motif were much less sensitive to substitution than were the histidines. The mutation of leucine 22 to alanine actually had a moderate, though significant, effect on the methionine activation reaction. Furthermore, the substitution of glycine 23 with an alanine had no significant consequence on the activation reaction nor on the overall $tRNA_f^{Met}$ aminoacylation reaction. Indeed, the k_{cat} and K_m values associated to $tRNA_f^{Met}$ were identical to those measured with the M547 wild-type control (data not shown). This result is rather surprising given that glycine is the only strictly invariant residue in all HIGH motifs of class I aaRS.

The two peptidic markers, HIGH and KMSKS, have constant positions within the nucleotide binding fold of class I aaRS (8–10,33,34). These two motifs lie in loops connecting constant secondary structure elements and are systematically located in the vicinity of the ATP binding crevice. The available biochemical studies dissecting the role of the KMSKS consensus sequence demonstrate that the corresponding basic residues are very important for achieving catalysis. The positive electric charges brought by these residues at neutral pH may dissipate the negative charges carried by the pyrophosphate moiety of the ATP molecule and, consequently, favour the attack of the α-phosphate of ATP by the carboxylate group of the aminoacid substrate. While the polar residues of the HIGH motif also appear to bind ATP, both peptides containing the motifs interact significantly with ATP only at the level of the transition state of the aminoacid activation reaction. Indeed, mutations of the corresponding residues have only a very small effect on the formation of the ground state ternary complex. Such a role implies that the loops containing these peptides are quite flexible. This was indirectly demonstrated with the KMSKS loops of TyrRS and MetRS (14,15). In the present study, the detrimental effect on the activity of *E.coli* MetRS resulting from the substitution of Gly23 with a proline further supports this idea.

To conclude, the available data show that the conserved HIGH and KMSKS sequences have concomittant positive actions during the formation and stabilization of the transition state. By examining the tertiary structure of the GlnRS–tRNA–ATP complex, the HIGH motif could be shown to interact with the KMSKS motif through a single hydrogen bonding between the main chain carboxylate

group of the methionine of KMSKS and the main chain amino group of the glycine of HIGH (8). Because GlnRS requires the presence of tRNA to activate glutamine, such a bridge, as deduced from the examination of a tRNA-containing GlnRS complex, might be representative of the transition state conformation occurring during glutaminyl-adenylate formation (35). A synergistic action of the two peptidic markers of class I aaRS can therefore be envisaged.

ACKNOWLEDGEMENTS

Thierry Meinnel is acknowledged for helpful advice. We are indebted to Victor Perlroth for critical reading of the manuscript.

REFERENCES

1 Eriani, G., Delarue, M., Poch, O., Gangloff, J. and Moras, D. (1990) *Nature (London)*, **347**, 203–206.
2 Cusack, S., Härtlein, M. and Leberman, R. (1991) *Nucleic Acids Res.*, **19**, 3489–3498.
3 Barker, D. G. and Winter, G. (1982) *FEBS Lett.*, **145**, 191–193.
4 Webster, T., Tsai, H., Kula, H. T. M., Mackie, G. A. and Schimmel, P. (1984) *Science*, **226**, 1315–1317.
5 Hountondji, C., Dessen, P. and Blanquet, S. (1986) *Biochimie*, **68**, 1071–1078.
6 Rossmann, M. G., Moras, D. and Olsen, K. W. (1974) *Nature (London)*, **250**, 194–199.
7 Ruff, M., Krishnaswamy, S., Boeglin, M., Poterszman, A., Mitschler, A., Podjarny, A., Rees, B., Thierry, J. C. and Moras, D. (1991) *Science*, **252**, 1682–1689.
8 Perona, J. J., Rould, M. A. and Steitz, T. A. (1993) *Biochemistry*, **32**, 8758–8771.
9 Brick, P., Bhat, T. N. and Blow, D. M. (1989) *J. Mol. Biol.*, **208**, 83–98.
10 Brunie, S., Zelwer, C. and Risler, J.-L. (1990) *J. Mol. Biol.*, **216**, 411–424.
11 Mechulam, Y., Dardel, F., LeCorre, D., Blanquet, S. and Fayat, G. (1991) *J. Mol. Biol.*, **217**, 465–475.
12 First, E. A. and Fersht, A. R. (1993) *Biochemistry*, **32**, 13644–13650.
13 First, E. A. and Fersht, A. R. (1993) *Biochemistry*, **32**, 13651–13657.
14 First, E. A. and Fersht, A. R. (1993) *Biochemistry*, **32**, 13658–13663.
15 Schmitt, E., Meinnel, T., Blanquet, S. and Mechulam, Y. (1994) *J.Mol.Biol*, **242**, 566–577.
16 Leatherbarrow, R. J. and Fersht, A. R. (1987) *Biochemistry*, **26**, 8524–8528.
17 Lowe, D. M., Fersht, A. R. and Wilkinson, A. J. (1985) *Biochemistry*, **24**, 5106–5109.
18 Borgford, T. J., Gray, T. E., Brand, N. J. and Fersht, A. R. (1987) *Biochemistry*, **26**, 7246–7250.
19 Chan, K. W. and Koeppe, R. E., II (1994) *Biochem. Biophys. Acta*, **1205**, 223–229.
20 Mellot, P., Mechulam, Y., LeCorre, D., Blanquet, S. and Fayat, G. (1989) *J. Mol. Biol.*, **208**, 429–443.
21 Fourmy, D., Meinnel, T., Mechulam, Y. and Blanquet, S. (1993) *J. Mol. Biol.*, **231**, 1068–1077.
22 Hirel, P.-H., Lévêque, F., Mellot, P., Dardel, F., Panvert, M., Mechulam, Y. and Fayat, G. (1988) *Biochimie (Paris)*, **70**, 773–782.
23 Meinnel, T., Mechulam, Y., LeCorre, D., Panvert, M., Blanquet, S. and Fayat, G. (1991) *Proc. Natl. Acad. Sci. USA*, **88**, 291–295.
24 Cassio, D. and Waller, J.-P. (1971) *Eur. J. Biochem.*, **20**, 283–300.
25 Blanquet, S., Fayat, G. and Waller, J. P. (1974) *Eur. J. Biochem.*, **44**, 343–351.
26 Blanquet, S., Fayat, G., Waller, J. P. and Iwatsubo, M. (1972) *Eur. J. Biochem.*, **24**, 461–469.
27 Blanquet, S., Petrissant, G. and Waller, J. P. (1973) *Eur. J. Biochem.*, **36**, 227–233.
28 Fayat, G., Fromant, M. and Blanquet, S. (1977) *Biochemistry*, **16**, 2570–2579.
29 Blanquet, S., Fayat, G. and Waller, J. P. (1975) *J. Mol. Biol.*, **94**, 1–15.
30 Dardel, F. (1994) *Comput. Applic. Biosci.*, **10**, 273–275.
31 Hyafil, F., Jacques, Y., Fayat, G., Fromant, M., Dessen, P. and Blanquet, S. (1976) *Biochemistry*, **15**, 3678–3685.
32 Meinnel, T., Mechulam, Y. and Blanquet, S. (1995) In D. Söll and U. RajBhandary (ed.), *tRNA: Structure, Biosynthesis, and Function*, ASM Press, Washington, DC, pp 251–292
33 Doublié, S., Bricogne, G., Gilmore, C. and Carter Jr, C. W. (1995) *Structure*, **3**, 17–31.
34 Nureki, O., Vassylyev, D. G., Katayanagi, K., Shimizu, T., Sekine, S., Kigawa, T., Miyazawa, T., Yokoyama, S. and Morikawa, K. (1995) *Science*, **267**, 1958–1965.
35 Ravel, J. M., Wang, S.-F., Heinemeyer, C. and Shive, W. (1965) *J. Biol. Chem.*, **240**, 432–438.
36 Kraulis, P. (1991) *J. Appl. Crystallogr.*, **24**, 946–950.